Highly Active Carbonaceous Nanofibers: A Versatile Scaffold for Constructing Multifunctional Free-Standing Membranes

Hai-Wei Liang,[†,§] Wen-Jun Zhang,[†,§] Yi-Ni Ma,[‡] Xiang Cao,[†] Qing-Fang Guan,[†] Wei-Ping Xu,[†] and Shu-Hong Yu[†,*]

[†]Division of Nanomaterials and Chemistry, Hefei National Laboratory for Physical Sciences at Microscale, Department of Chemistry, National Synchrotron Radiation Laboratory, University of Science and Technology of China, Hefei, Anhui 230026, China and [‡]School of Pharmacy, Anhui University of Traditional Chinese Medicine, Hefei 230038, China [§]These two authors contributed equally to this work.

ABSTRACT Translating the unique characteristics of individual nanoscale components into macroscopic materials such as membranes or sheets still remains a challenge, as the engineering of these structures often compromises their intrinsic properties. Here, we demonstrate that the highly active carbonaceous nanofibers (CNFs), which are prepared through a template-directed hydrothermal carbonization process, can be used as a versatile nanoscale scaffold for constructing macroscopic multifunctional membranes. In order to demonstrate the broad applicability of the CNF scaffold, we fabricate a variety of CNF-based composite nanofibers, including CNFs-Fe_3O_4, CNFs-TiO_2, CNFs-Ag, and CNFs-Au through various chemical routes. Importantly, all of them inherit unique dimensionality (high aspect ratio) and mechanical properties (flexibility) of the original CNF scaffolds and thus can be assembled into macroscopic free-standing membranes through a simple casting process. We also demonstrate the wide application potentials of these multifunctional composite membranes in magnetic actuation, antibiofouling filtration, and continuous-flow catalysis.

KEYWORDS: carbonaceous nanofibers · free-standing membranes · multifunctional · assemble · antibiofouling filtration · continuous-flow catalysis

With the fast development of nanotechnology during the past two decades, especially in synthetic aspect, high-quality nanomaterials with various compositions and dimensions have been fabricated successfully through different physical and chemical strategies. Although the properties of nanomaterials are frequently superior to those of their bulk counterparts, translating the unique characteristics of individual nanoscale components into macroscopic materials still remains a challenge. On the other hand, it is attractive to integrate two or more kinds of nanomaterials into single units, which enables the creation of multifunctional materials with new or improved properties. One important technological thrust is the development of highly efficient and scalable assembly methods to fabricate functional devices with specific properties.[1] Equally intriguing is exploring versatile scaffolds on which other components with desirable functionalities can easily be built in nanoprecision.[2]

One-dimensional nanomaterials (1D), special carbon nanotubes (CNTs), have been widely used as nano-building blocks for generating a range of macroscopic structures, including films,[3] sheets,[4] membranes,[5] and aerogels.[6] CNTs have also served as efficient platforms for building multifunctional composite materials.[7,8] However, the harsh synthetic routes and poor functionalized surfaces of CNTs have hindered the manufacture of CNT-based materials. Recently, a few other 1D nanostructures, such as metal oxide[9,10] and hydroxide nanowires,[11] electrospun fibers,[12,13] cellulose nanofibers,[2,14,15] and polymer,[16] have been employed as blocks or platforms to generate macroscopic materials for various applications. Although some of them, for example, cellulose nanofibers, have shown obvious advantages such as easy availability in large quantities from biomass,[15] it is difficult to manipulate their sizes (diameters) and surface functionalities, which are crucial for the fabrication feasibility and the performance of the final products. Therefore, it is desirable to develop a versatile nanoscale scaffold to easily construct multifunctional macroscopic materials.

In our previous work, we reported a new type of free-standing and robust membrane consisting of highly uniform and active carbonaceous nanofibers (CNFs),[17] which were prepared by the template-directed hydrothermal carbonization (HTC) process.[18] In this article, we demonstrate that the CNFs can serve as excellent platforms on which

* Address correspondence to shyu@ustc.edu.cn.

Received for review July 23, 2011 and accepted September 20, 2011.

Published online September 20, 2011
10.1021/nn202789f

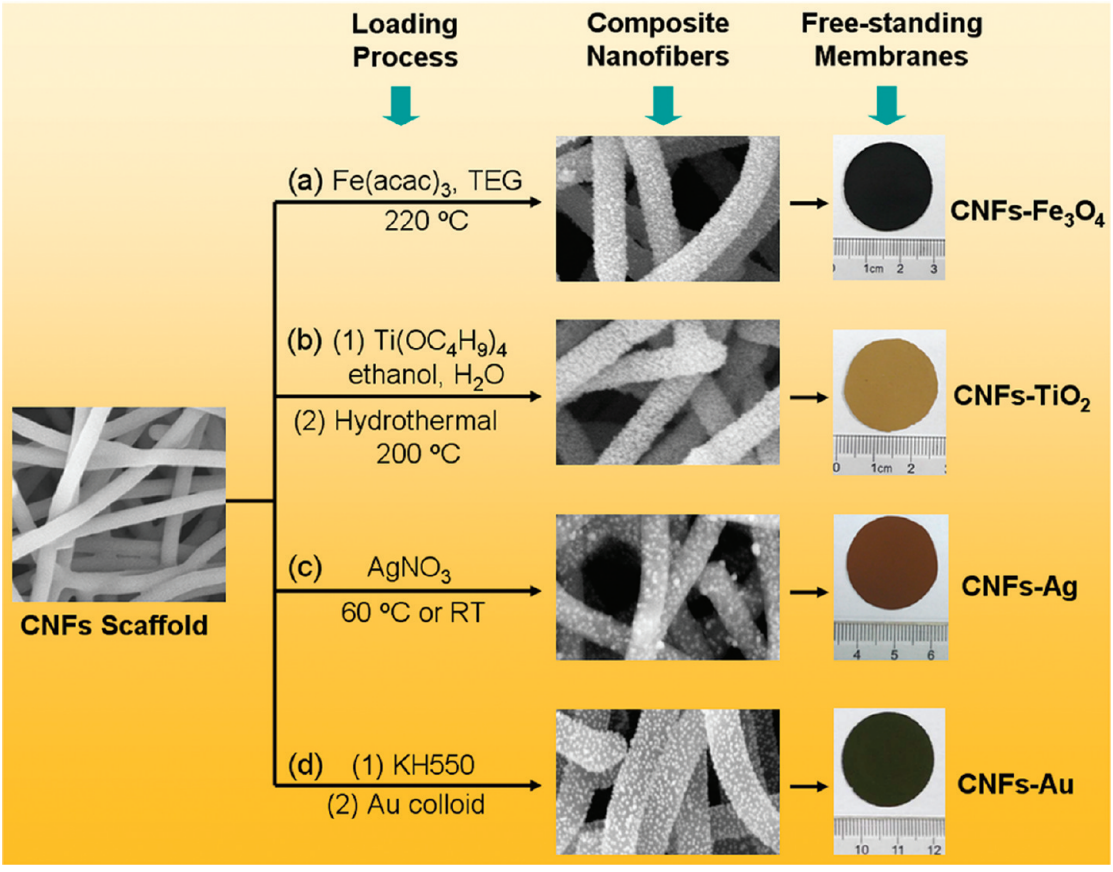

Scheme 1. Schematic illustrations showing the broad versatility of the CNF scaffolds for constructing free-standing multifunctional membranes, including (a) CNFs-Fe_3O_4, (b) CNFs-TiO_2, (c) CNFs-Ag, and (d) CNFs-Au.

other components with desirable functionalities are built. Compared with other 1D nanoscale scaffolds, the CNFs have three significant advantages for constructing macroscopic functional materials, namely, (i) highly functionalized surfaces, (ii) controllable fiber size (diameter of CNFs), and (iii) easy handling for assembling them into free-standing membranes. Our previous studies indicated that the CNFs obtained by the HTC process were highly functionalized with abundant hydroxylic and carboxylic groups.[18] Thus, the surface of CNFs is hydrophilic and can be well-dispersed in water,[17,19] which facilitates the modification of them with given chemicals or nanoparticles. The presence of carboxylic groups makes the CNFs negatively charged and bind directly with metal ions or nanoparticles with opposite charges by electrostatic attractions. Besides, the oxygen-containing groups on the surface of CNFs have remarkable reducing ability for *in situ* loading with noble metal nanoparticles;[19] also, they can react with various organic chemicals (such as silanes) in the gaseous or solvent phase to yield preferably monolayers with the desired functionality.[20] Overall, the highly functionalized surfaces of CNFs allow for easy loading of various nanoparticles on them through different chemical routes. Furthermore, the obtained composite nanofibers inherit unique dimensionality (high aspect ratio) and mechanical properties (high flexibility) of the original CNF scaffolds and thus can be assembled into robust membranes. Finally, we can precisely control the diameter of CNFs from only a few tens to hundreds of nanometers by simply regulating the HTC reaction time. All of these different sized CNFs have similar surface characteristics and can be incorporated with functional materials to form composite nanofibers with different sizes. Therefore, the CNF-based membranes with the desirable physical and chemical properties and functionalities can be available according to the requirements of practical applications.

Herein, benefiting from the unique advantages of the CNF scaffolds, we can prepare a series of multifunctional fibrous composite membranes, including CNFs-Fe_3O_4, CNFs-TiO_2, CNFs-Ag, and CNFs-Au through various chemical processes (Scheme 1). We demonstrate the versatility of the CNF scaffolds by regulating the composition, loading, and size of particles loaded and the diameters of CNFs, as well as their magnetic, optical, antimicrobial and antifouling, and catalytic functionalities of these CNF-based composite membranes.

RESULTS AND DISCUSSION

The highly uniform CNFs were first fabricated through the template-directed hydrothermal carbonization (HTC)

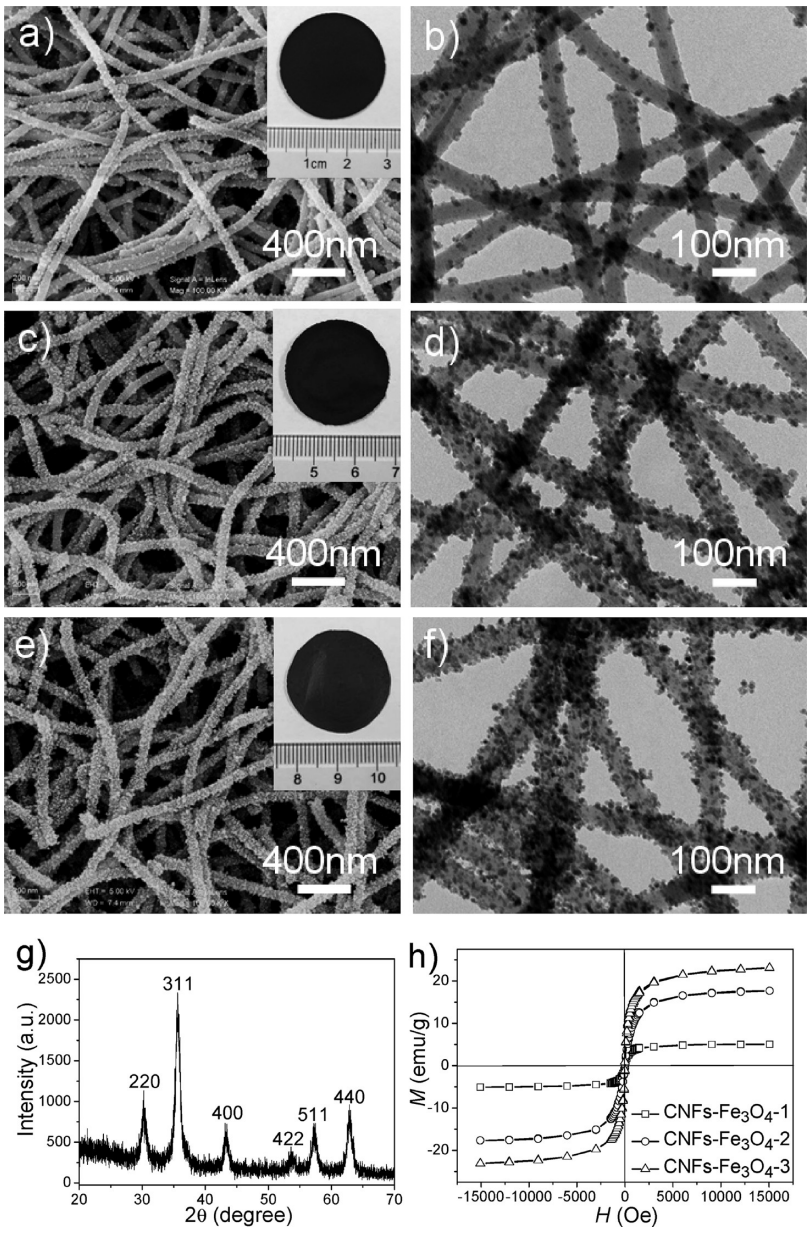

Figure 1. Morphology, phase, and magnetic characterization of CNFs-Fe_3O_4 composite nanofibers. (a–f) SEM and TEM images of CNFs-50-Fe_3O_4-1 (a,b), CNFs-50-Fe_3O_4-2 (c,d), and CNFs-50-Fe_3O_4-3 (e,f), which were fabricated by thermal decomposition of 100, 200, and 400 mg of $Fe(acac)_3$ in the presence of 100 mg of CNFs-50 in TEG, respectively. The insets in the SEM images show the photographs of the corresponding CNFs-Fe_3O_4 membranes. (g) XRD pattern of the CNFs-50-Fe_3O_4-2 sample. (h) Room-temperature magnetic hysteresis loops of the three CNFs-Fe_3O_4 samples.

processes using ultrathin Te nanowires as templates and glucose as the carbon source.[17,18] The diameter of CNFs could be well controlled from tens to hundreds of nanometers by simply regulating the HTC time and the ratio of Te templates to glucose.[17] In the present work, we fabricated three different sized CNF scaffolds, namely, CNFs-50, CNFs-130, and CNFs-200 (the number represents the average diameters of the CNFs (nm)) by HTC reaction at 160 °C for 18, 60, and 72 h, respectively (see Supporting Information, Figure S1). Furthermore, these highly uniform CNFs with a length up to hundreds of micrometers are very flexible, making it possible to use CNFs as scaffolds for constructing free-standing nanofibrous composite membranes. In order to demonstrate the versatility of our CNF scaffolds, we prepared a series of composite nanofibers through various chemical processes (Scheme 1). The sample description and details of synthetic parameters are summarized in Table S1. The pure CNFs and CNF-based composite nanofibers were then assembled into corresponding membranes by a simple casting process.[17]

CNFs-Fe_3O_4 Nanofibrous Membranes as Magnetic Actuators. We first demonstrated the versatility of the CNF scaffolds by constructing a free-standing magnetic membrane. Magnetite Fe_3O_4 nanoparticles show their unique magnetic and electric properties, which lead

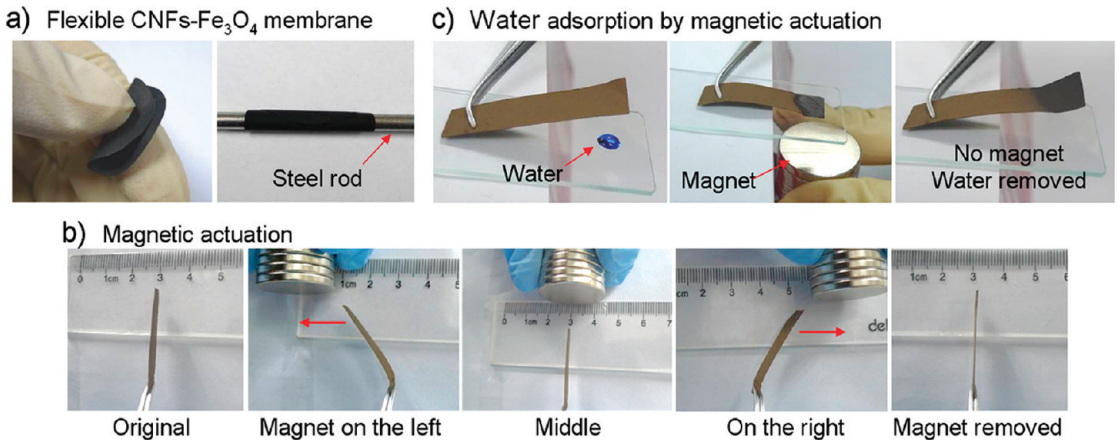

Figure 2. (a) Demonstration of the flexibility of the as-prepared CNFs-50-Fe_3O_4-2 composite membranes. (b) Composite membrane (CNFs-130-Fe_3O_4) could be actuated by a simple household magnet and exhibit reversible and large deformation. (c) Magnetic membrane (CNFs-130-Fe_3O_4) bends downward in response to the magnet to absorb the water droplet on the glass substrate. It retains its original place upon removal of the magnet. The water droplet was labeled with methylene blue for clear presentation.

to broad applications in high-density information storage, electronic devices, ferrofluid technology, *etc.*[21−23] Herein, we prepared the CNFs-Fe_3O_4 composite nanofibers through thermal decomposition of $Fe(acac)_3$ in triethylene glycol (TEG) in the presence of CNFs (Scheme 1a). Figure 1 shows the morphology, phase, and magnetic characterization of the three CNFs-Fe_3O_4 samples synthesized from CNFs-50. The XRD pattern of the product shows that all of the diffraction peaks can be indexed as a pure cubic spinel crystal structure of magnetite (Figure 1g). The SEM and TEM images show that all of the CNFs were uniformly coated with ~8 nm magnetite nanoparticles, and no aggregated or free nanoparticles in the solution were found (Figure 1a−f). It has been found that the coverage density of magnetite nanoparticles on CNFs can be easily tuned by changing the $Fe(acac)_3$ concentration and the initial weight ratio of $Fe(acac)_3$:CNFs. For example, the Fe_3O_4 nanoparticles are widely spaced on CNFs when the weight ratio of $Fe(acac)_3$:CNFs is 1:1 (Figure 1a,b), whereas the nanoparticles are more densely distributed and the loading is at saturation when the weight ratio increases to 4:1 (Figure 1e,f). Inductively coupled plasma atomic emission spectrometry (ICP-AES) analysis indicated that the contents of Fe_3O_4 in final products increased gradually from 6.8 (CNFs-50-Fe_3O_4-1) to 12.5 (CNFs-50-Fe_3O_4-2) and 16.2 wt % (CNFs-50-Fe_3O_4-3) with the increase of the $Fe(acac)_3$:CNFs weight ratio.

The formation mechanism of magnetite nanoparticles on the surface of CNFs was believed to be similar to that of decoration of Fe_3O_4 on CNTs or graphene.[24,25] $Fe(acac)_3$ was first decomposed and partly reduced by TEG into magnetite tiny particles that possessed high surface energy and were preferentially adsorbed onto the surface of CNFs from polyol solution, which was confirmed by the TEM observation of the intermediate products at the early stage of the reaction (see Supporting Information, Figure S2). These unstable tiny particles tended to aggregate and grow by the interaction of van der Waals forces and magnetic dipole. Finally, when these particles grew to a critical size, they were stabilized with TEG and formed the uniform magnetite nanoparticles decorating the CNFs.[24,25]

Magnetic measurements were carried out on the three as-prepared CNFs-Fe_3O_4 samples. The magnetization curves show that all of the three composites with various loading amounts of Fe_3O_4 nanoparticles exhibited superparamagnetic behavior at room temperature with no coercivity or remanence (Figure 1h and Figure S3). This is consistent with the nanoparticle size of Fe_3O_4 (~8 nm), which is in the superparamagnetic size range.[25] The saturation magnetizations of the three CNFs-Fe_3O_4 samples are 5.2, 17.8, and 22.9 emu·g^{-1}, corresponding to the samples prepared with the initial weight ratio of $Fe(acac)_3$:CNFs of 1:1, 2:1, and 4:1, respectively. The results revealed that the magnetic properties of CNFs-Fe_3O_4 composite nanofibers can be finely tuned by controlling the loading amount of magnetite nanoparticles on the CNF matrix through changing reaction conditions.

Furthermore, we have also decorated magnetite particles on the other two CNFs scaffolds, that is, CNFs-130 and CNFs-200, to form corresponding composite nanofibers (see Supporting Information, Figure S4 and Table S1). All of these CNFs-Fe_3O_4 composite nanofibers can be easily assembled into free-standing magnetic membranes through the casting process (insets in the SEM images in Figure 1 and Figure S4). Especially, these magnetic membranes were strikingly flexible and mechanically stable (Figure 2a), although the mechanical strength has not been examined quantitatively. The present flexibility can be explained by the unique network structure of the CNF-based membrane, in which high aspect ratio nanofibers are very flexible and highly entangled with each other. Another unique property of the CNFs-Fe_3O_4 composite

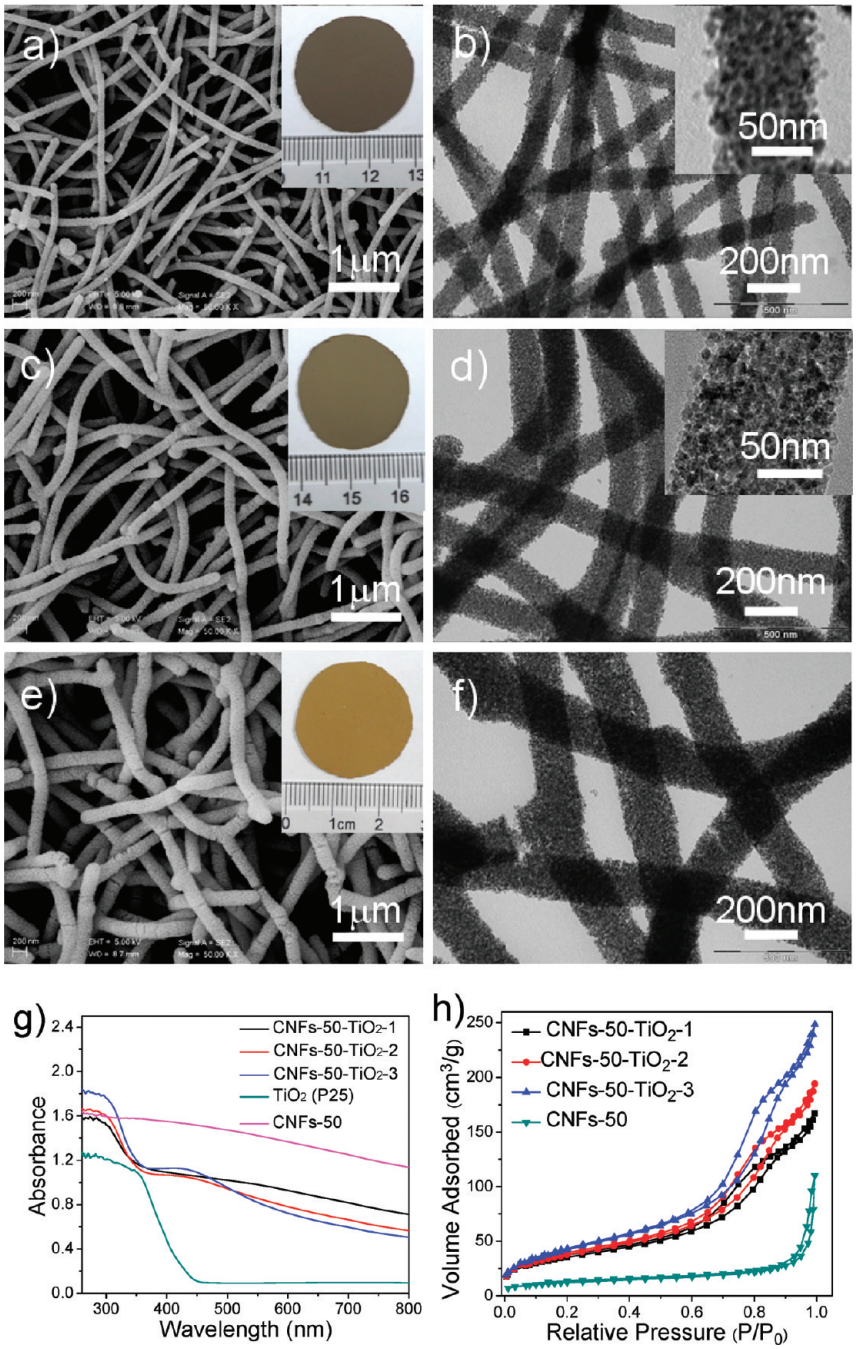

Figure 3. Morphology, absorption spectra, and BET characterizations of the CNFs-TiO_2 composites. (a–f) SEM and TEM images of CNFs-50-TiO_2-1 (a,b), CNFs-50-TiO_2-2 (c,d), and CNFs-50-TiO_2-3 (e,f), which were fabricated through the sol–gel and subsequent hydrothermal processes. The insets in the SEM images show the photographs of the corresponding free-standing membranes. The insets in (b) and (d) are the corresponding high-magnification TEM images. (g) Diffuse reflectance absorption spectra of the as-prepared CNFs-TiO_2 composite membranes and the pure CNFs-50 membrane and TiO_2 (P25) in comparison. (h) Nitrogen adsorption–desorption isotherms of pure CNFs-50 and the CNFs-TiO_2 composite membranes.

membrane is that it can be actuated by a small magnetic field. Figure 2b shows that a simple household magnet can provide reversible and large deformation of the CNFs-Fe_3O_4 membrane without any cracks. There was no apparent damage even after 100 repeated bending cycles under the actuation of the magnet. Such magnetic composite membranes also can maintain their mechanical and magnetic stability after storing them at atmospheric conditions for half a year. Benefiting from their sensitive magnetic response and high porosity, the CNFs-Fe_3O_4 membrane could be magnetically actuated to absorb the droplet of water on the glass substrate and recover to its original place after the removal of the magnet (Figure 2c).

Overall, we have opened up the availability of a functionalized CNF matrix with magnetic nanoparticles

TABLE 1. Textural Properties of Pure CNFs and CNFs-TiO_2 Composite Membranes

samples	TiO_2 loading (wt %)	S_{BET} ($m^2\ g^{-1}$)	V_{total} ($cm^3\ g^{-1}$)	D (nm)
CNFs-50-TiO_2-1	28.9	128.9	0.22	6.8
CNFs-50-TiO_2-2	44.2	138.5	0.26	7.2
CNFs-50-TiO_2-3	59.8	157.7	0.34	8.7
CNFs-50	0	41.9	0.17	23.2

to form a new class of nanofibrous membrane with unique magnetic and mechanical properties, which are expected to be useful in various fields such as electromagnetic actuators, smart microfluidics devices, and biomedicine.

CNFs-TiO_2 Nanofibrous Membranes. We further showed the versatility of the CNF scaffolds by constructing free-standing membrane-carrying photocatalysts, such as TiO_2 nanoparticles. Due to its cheap, nontoxic, and highly efficient photocatalytic properties, TiO_2 has attracted a lot of attention and its applications in degradation of organic pollutants, air purification, sterilization, and energy conversion have been widely studied.[26−28] Herein, we prepared CNFs-TiO_2 composite nanofibers through sol−gel and hydrothermal processes and subsequently assembled them into free-standing fibrous membranes (Scheme 1b). The CNFs were first coated with a layer of amorphous titanium oxide (or hydroxide) to form the core/shell 1D nanostructures (see Supporting Information, Figure S5a) through a sol−gel process using tetrabutyltitanate as the precursor. According to the previous study, the CNFs are highly functionalized with oxygen groups,[18] which can capture a metallic precursor through coordination or electrostatic interaction. Thus, amorphous titanium oxide (or hydroxide) was preferentially formed on the surface of CNFs to yield the core/shell nanostructures. After hydrothermal treatment at 180 °C for 12 h, the highly porous CNFs-TiO_2 composite nanofibers were obtained (Figure S5b). XRD technique indicated that the amorphous core/shell nanostructures have been successfully converted into crystalline CNFs-TiO_2 (anatase phase) nanofibers by hydrothermal treatment (Figure S5c). Figure 3a−f shows the SEM and TEM images of three CNFs-TiO_2 composite nanofibers fabricated by coating various amounts of TiO_2 on CNFs-50. In detail, coating 0.1, 0.2, and 0.4 mL of tetrabutyltitanate on 50 mg of CNFs-50 can yield CNFs-TiO_2 composite nanofibers with diameters of 78, 115, and 172 nm, respectively (Figure 3a−f). The high-magnification TEM images indicate that the coating layers of these composite nanofibers consist of abundant tiny TiO_2 nanoparticles with a size of 5−10 nm (the insets in Figure 3b,d). The ICP-AES technique revealed that the TiO_2 contents in the three composites are 28.9 (CNFs-50-TiO_2-1), 44.2 (CNFs-50-TiO_2-2), and 59.8% (CNFs-50-TiO_2-3) (Table 1). Similarly, the CNFs with larger diameter can also be well coated with TiO_2 nanoparticles through the sol−gel and hydrothermal processes (see Supporting Information, Figure S6).

All of these prepared CNFs-TiO_2 composite nanofibers can be assembled into corresponding free-standing membranes (insets in the SEM images in Figure 3 and Figure S6). Interestingly, the color of the composite fibrous membranes became lighter with the increase of TiO_2 loading. The optical properties of the CNFs-TiO_2 composite membranes were investigated by the UV−vis diffuse reflectance absorption spectra (Figure 3g). All of the CNFs-TiO_2 samples and commercially available pure TiO_2 (P25) show the typical absorption with an intense transition in the UV region of the spectra due to electron promotion of TiO_2 from the valence band to the conduction. Compared with pure TiO_2, the CNFs-TiO_2 composite membranes showed significant enhancement of light absorption in the wavelength range of 400−800 nm due to the presence of the carbonaceous component in the composite. Furthermore, the absorbance of the composites in the UV region was enhanced with the increase of the TiO_2 content, while their absorbance in the visible region decreased gradually, which is consistent with the color change of these composite membranes.

We further examined the textural nature of the CNFs-TiO_2 composite membranes by the N_2 adsorption−desorption isotherms (Figure 3h and Table 1). The remarkable hysteresis loops indicate the mesoporous nature of these composite membranes (Figure 3h). After loading of TiO_2 nanoparticles with a size of 5−10 nm on the CNFs, abundant mesopores formed between TiO_2 nanoparticles, thus resulting in higher BET surface areas than pure CNF membranes (Table 1). With the increase of loading amount of TiO_2, the percentage of CNFs in the composites decreases and the mesoporous feature becomes pronounced gradually (Figure 3h). The mean pore sizes of the composite membranes are in the range of 6−9 nm (Table 1), which are dominantly contributed from the pores between TiO_2 nanoparticles on CNFs and agree with the results of TEM observations (Figure 3).

In short, we have achieved the construction of TiO_2-containing functional nanofibrous membranes by using the CNF scaffolds. Benefiting from the mechanical stability of the nanofibrous composite membrane and the potential photocatalytic ability, we envisage their potential application in highly efficient sterilization and organics degradation by integrating the filtration and photocatalytic process.[29,30] Besides the CNFs-TiO_2 composites demonstrated here, it can be inferred that other functional metal oxides, such as SnO_2, ZrO_2, SiO_2, and ZnO, can also be rapidly loaded on the CNF scaffolds through the sol−gel processes using corresponding metal organic precursors.

CNFs-Ag Nanofibrous Membranes with Antimicrobial Functionality Used as High-Performance Filters: Preventing Biofilm Formation. Membrane processes, such as reverse osmosis,

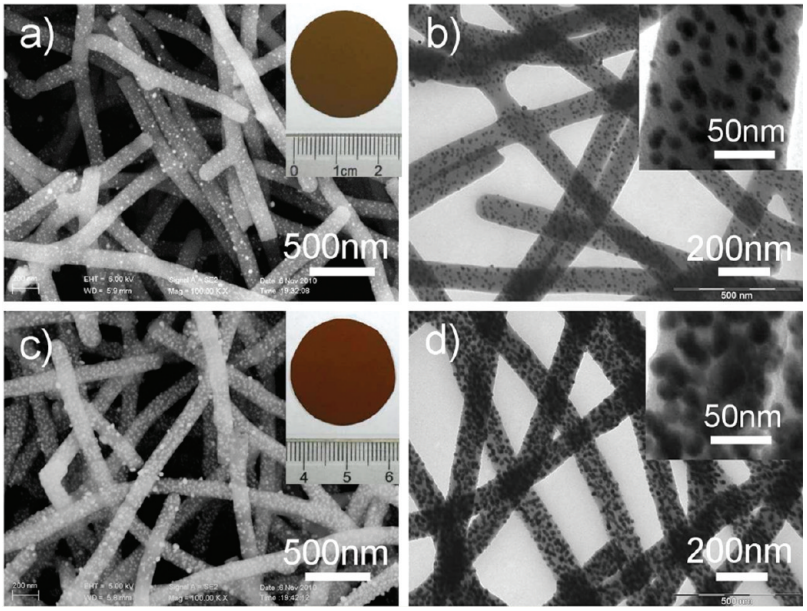

Figure 4. Morphology characterization of CNFs-Ag composite nanofibers. (a,c) SEM and (b,d) TEM images of CNFs-130-Ag-1 (a,b) and CNFs-130-Ag-2 (c,d) fabricated by *in situ* reduction of $AgNO_3$ at room temperature and 60 °C, respectively. The insets in (a,c) show the photographs of the corresponding CNFs-Ag membranes. The insets in (b) and (d) are the corresponding high-magnification TEM images.

microfiltration, and nanofiltration, are more and more important in acquiring safe and potable water.[31,32] However, biological fouling or biofilm formed by a surface-associated layer of microorganisms seriously deteriorated the membrane performance.[33,34] Biofouling is extraordinarily difficult to control because even a few bacteria on a membrane surface can finally multiply to form biodetrimental films. Besides, waste produced by the organisms in a biofilm may damage the filtration membranes and perhaps cause microbial contamination of permeate.[35] Therefore, there is a strong demand for a filtration membrane with antifouling functionality to reach perfect achievements in water treatment. Here, we fabricated a novel type of CNFs-Ag composite membranes through *in situ* reduction of $AgNO_3$ by hydroxylic groups on CNFs (Scheme 1c). Silver has long been known to exhibit high antibacterial properties as well as low toxicity for human cells.[36] Additionally, the use of CNFs as a matrix for fixation of Ag nanoparticles efficiently prevents the aggregation of nanoparticles and permits control over the sizes of nanoparticles. Embedding silver nanoparticles in the CNF matrix puts on a perfect performance in inhibiting the growth and proliferation of microbes. Importantly, more than just filtrating out the bacteria from water, the as-prepared composite fibrous membrane could effectively prevent the biofilm formation, which is crucial to make filters maintain a high performance for long-term.

The XRD pattern of the as-prepared product shows that all peaks can be indexed to *fcc* silver (see Supporting Information, Figure S7). Abundant Ag nanoparticles (AgNPs) were compactly and uniformly distributed in the CNF matrix, as shown in the SEM and TEM images (Figure 4). Except for a small percentage of AgNPs on the surface of the CNFs, the vast majority of AgNPs were embedded inside the CNF matrix. This could be more clearly observed in the TEM images in Figure 4b,d (insets), which show particularly smooth edges of the CNFs-Ag composite nanofibers. Although the detailed formation process is not been fully understood at present, the unique physical and chemical properties of CNFs were believed to play a key role in the formation of this Ag-embedded structure. The formation mechanism of CNFs-Ag here is obviously different from that of CNFs-Fe_3O_4 and CNFs-TiO_2 described above, where the CNF matrix was only used as a support. In the formation process of CNFs-Ag composite nanofibers, the CNFs served not only as scaffolds for Ag loading but also as reducing agents for reducing of Ag^+ and subsequent formation of Ag nanoparticles because the oxygen-containing groups in the CNF matrix possess remarkable reducing ability for *in situ* loading with noble metal nanoparticles.[19] Furthermore, it is believed that these oxygen-containing groups with reducibility are uniformly distributed both on the surface and inside the CNF matrix. Our previous studies revealed that the carbonaceous matrix obtained from the low-temperature HTC process allowed for free diffusion of ionic reactants.[37] Therefore, Ag^+ ions could diffuse into the interior of CNFs freely and then were reduced to Ag nanoparticles, which were stabilized by the surrounding carbonaceous matrix. The Ag nanoparticles formed on the surface of CNFs at an early stage were relatively active and probably disappeared as a result of the Ostwald ripening process. The control experiment, in which another reducing agent such as

hydrazine hydrate or ethylene glycol was involved, showed that larger Ag nanoparticles formed on the surface of CNFs (see Supporting Information, Figure S8). Thus, we believed that the specific physical and chemical properties of CNFs resulted in the unique Ag-embedded nanostructure. It is worthy to point out that this Ag-embedded structure allows for the release of sufficient antimicrobial component (Ag^+) for microbial control while preventing a rapid loss of antibiofouling activity resulting from depletion of silver from the membrane surface.[38]

The loading and size of AgNPs in the CNF matrix could be easily controlled by regulating the reducing temperatures. For example, *in situ* reducing of $AgNO_3$ on the CNFs at room temperature gave 8.5 wt % Ag loading and ~10 nm AgNPs, while reaction at an elevated temperature (60 °C) resulted in 20.2 wt % loading and ~15 nm AgNPs (Figure 4b,d). A reasonable explanation is that the reducing ability of hydroxylic groups in CNFs is enhanced with the increase of reaction temperatures and leading to a higher Ag loading and larger AgNPs. Moreover, two other CNFs with different diameters, namely, CNFs-50 and CNFs-200, have also been *in situ* loaded with AgNPs to form composite nanofibers (see Supporting Information, Figure S9). These CNFs-Ag hybrid nanofibrous products could easily be assembled into corresponding free-standing membranes through the casting processes (insets in Figure 4a,c and Figure S9a,c), which are all mechanically strong enough for filtration operations, even under a pretty high pressure of 40 kPa. In short, various CNFs-Ag functional membranes with different antimicrobial and filtration properties can be available by controlling the size of AgNPs, loading, and the diameter of CNF scaffolds.

We chose the CNFs-130-Ag-2 membrane to evaluate the antibacterial and antibiofouling properties through several different aspects, although other CNFs-Ag products also exhibited antibacterial activity.

Bacterial Growth Kinetics. A common pollutant of drinking water is the faecal bacterium *Escherichia coli*, which is responsible for many waterborne diseases. We first quantitatively evaluated the antibacterial activity of the CNFs-Ag composite nanofibers by studying the *E. coli* growth kinetics in LB liquid media. *E. coli* was incubated in a growth medium containing various concentrations of CNFs-Ag or pure CNF samples, and the change of optical density of the medium with incubation time was measured using a UV−vis spectrophotometer at 600 nm. Figure 5a shows the results of the CNFs-Ag composite nanofibers against *E. coli*. In contrast with the rapid growth of bacteria in the control and pure CNF solution, the growth of *E. coli* was completely inhibited during the whole 8 h culture period in the medium containing 50 and 100 μg/mL CNFs-Ag composites, whereas the absorbance of the medium containing 25 μg/mL CNFs-Ag composites

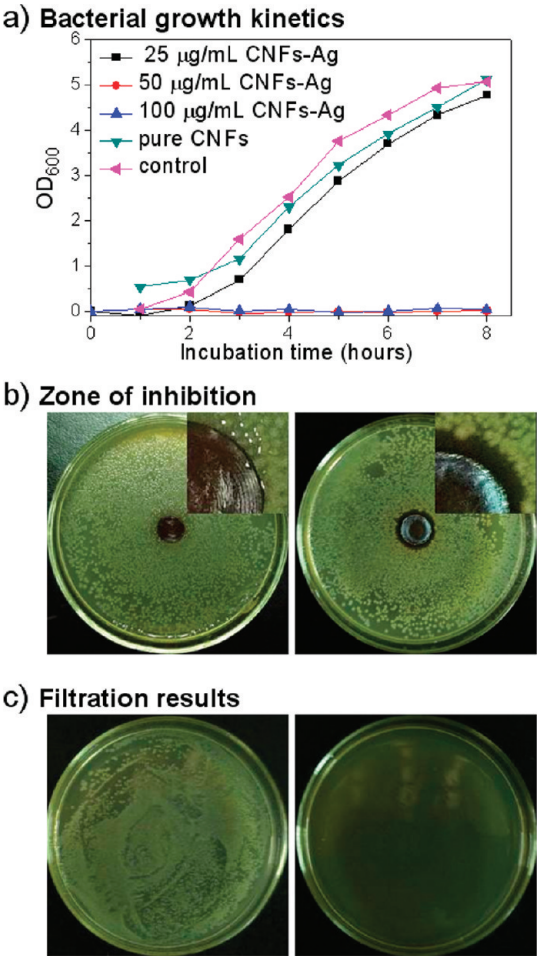

Figure 5. Antimicrobial activities and filtration properties of CNFs-Ag composite membranes against E. coli. (a) Bacterial growth curves in LB media with different amounts of CNFs-Ag composites and Ag-free CNFs. (b) Optical images of the zone of inhibition for Ag-free CNF membrane (left panel) and CNFs-Ag composite membrane (right panel). Each membrane is 8 mm in diameter. Incubation conditions: 37 °C, 24 h. (c) Filtration results for E. coli using the CNFs-Ag membrane. Left panel: the colonies of E.coli bacteria grown by the culture of the unfiltered solution. Right panel: the filtrate after culture showing the absence of the bacterial colonies.

increased with incubation time. These results confirmed the obvious antibacterial activity of the CNFs-Ag composite nanofibers against *E. coli* and the minimum inhibitory concentration was 50 μg/mL.

Zone of Inhibition. In order to investigate the intrinsic chemical antibacterial strength of the CNFs-Ag composites, the Kirby−Bauer method was employed. LB agar plates were prepared and inoculated with *E. coli*, and then the CNFs-Ag composite membrane and Ag-free CNF membrane were gently placed on the lawn of *E. coli* in the plates. After inoculation for 24 h, the CNFs-Ag composite membrane on the *E. coli*-inoculated surfaces inhibited the growth and multiplication of all the bacteria around them, and a distant inhibition zone (the clear areas with no bacteria growth) of about 2 mm around the membranes was

TABLE 2. Filtration and Antibiofouling Properties of the CNFs-130-Ag, CNFs-130, and Commercially Available MCE and PVDF Microfiltration Membranes

membrane samples	CNFs-130-Ag-2	CNFs-130	MCE[a]	PVDF[a]
thickness (μm)	50	50	140	110
pure water flux (L h^{-1} m^{-2})[b]	4560	4620	3450	1510
flux after fouling (L h^{-1} m^{-2})[b]	4340	150	52	35
flux after water rinse (L h^{-1} m^{-2})[b]	4370	2220	730	415

[a] Commercially available mixed cellulose ester (MCE) and polyvinylidene fluoride (PVDF) membrane, cutoff size = 0.1 μm, Shanghai Xingya Purification Materials Co. Ltd., China. [b] The flux was calculated as an average rate for the first 10 mL. A pressure of 40 kPa was applied by a N_2 tank.

observed (the right panel of Figure 5b). In contrast, the pure CNF membrane showed no antimicrobial activity as the large area of bacterial growth lawn was obvious everywhere on the agar plate (the left panel of Figure 5b). The above results indicated that the antimicrobial activity of the CNFs-Ag composite was primarily due to the release of Ag^+ from the CNFs matrix. Although the detailed mechanism of the antibacterial effect of silver nanoparticles is still insufficiently understood, many researchers reported that the release of Ag^+ played an essential role in antibacterial action. Ag^+ can bind to the electron donor groups containing sulfur, oxygen, or nitrogen and bring about structural and functional changes in the cells.[39] For instance, when Ag^+ binds to the proteins on the cell wall, the wall will be damaged and soon rupture, and then the internal cell content leaks out, leading to the death of the bacteria cell.[40]

Filtrating out Bacteria from Water. The CNFs-Ag composite membrane with a thickness of ~50 μm was then tested for its ability to remove microbial pathogens from water. After passing sterile saline water with light bacterial suspension (*E. coli*, ~10^6 CFU/mL) through the CNF-Ag nanofibrous membrane, both the unfiltered and filtered water were cultured on LB agar plates to check the efficiency of the filtration process. No bacteria colony appeared in the filtered product after incubation at ~37 °C overnight, whereas the bacterial colonies could be seen everywhere in the plate of unfiltered solution (Figure 5c). The results revealed that the CNFs-Ag composite membranes prepared here could successfully hold back the bacteria, leaving the filtered water free of bacteria and drinkable. In fact, it is not surprising that our membrane could filter out bacteria completely from water because the cutoff size of the CNF-based membranes is in the range of nanoscale or submicroscale[17] while the *E. coli* has a typical length of 2000 to 5000 nm and a width of 400 to 600 nm.

Biofilm-Controlling Effect. To obtain a valuable membrane filtration process for water treatment, requirements of preventing biological fouling and biofilm formation must be satisfied.[34] In order to evaluate the antibiofouling properties, the CNFs-Ag composite membrane was fouled by filtration of *E. coli* and incubating on the surface of LB agar plates. The pure

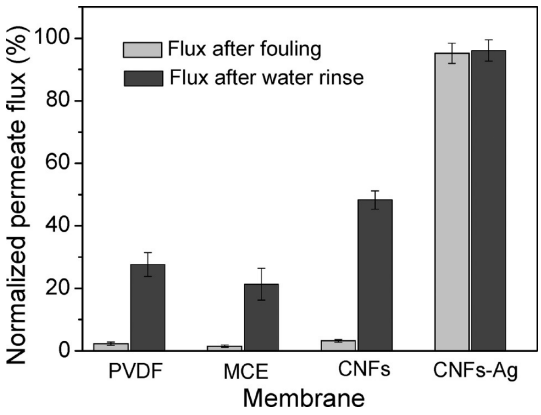

Figure 6. Filtration characteristics of the CNFs-130-Ag, CNFs-130, and commercially available MCE and PVDF microfiltration membranes at different stages. The permeate flux of each membrane at various stages was normalized to that of the corresponding membrane before fouling.

water flux was measured before and after fouling and after successive water rinsing. Ag-free CNF membranes, commercially available as mixed cellulose ester (MCE) and polyvinylidene fluoride (PVDF) membranes, were also tested as described above for comparison. The results are summarized and shown in Table 2. The pure water flux of the CNFs-Ag and Ag-free CNF membranes before fouling is obviously larger than that of the two commercially available membranes (Table 2), probably due to the thinness, hydrophilic properties, and the unique nanofibrous network structures of the CNF-based membranes.[17] More importantly, compared with the three other membranes, CNFs-Ag composite membrane showed fantastic antibiofouling properties (Table 2 and Figure 6). After fouling, the filtration rate of PVDF, MCE, and Ag-free CNF membrane dropped 97.7, 98.5, and 96.8%, respectively, which suggested that the biofilm has formed on the surfaces of the three membranes and almost completely blocked the pores of the membranes. Even after water rinse, the flux of the three membranes could never return to their original level (Figure 6). In contrast, the flux of CNFs-Ag composite membrane declined only a little, maintaining 95.2% of the original filtration rate after fouling (Figure 6). We further certified the antibiofouling behaviors of the CNFs-Ag composite membrane by SEM observations (Figure 7). There were lots of open pores in these membranes before filtration of bacteria solution (Figure 7a–d). However, after fouling and water rinse, many bacterial cells adhered tightly on the surface or inside the pores of the Ag-free and commercial membranes and could not be separated away even by hard hydraulic cleaning (Figure 7e–g), which greatly reduced their potential to effectively filter bacteria-containing water. In contrast, almost no bacteria cells were spotted over the entire surface of the fouled-cleaned CNFs-Ag composite membrane, indicating that the *E. coli* could not grow at all on the composite membrane.

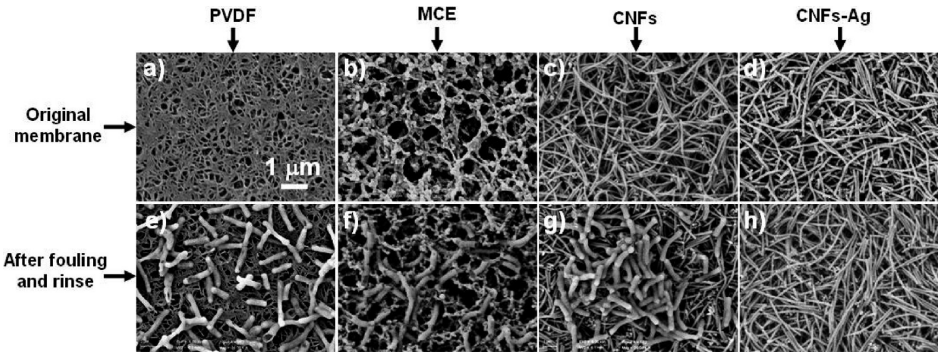

Figure 7. SEM images showing top surface of original membranes before fouling (a–d) and after fouling and hydraulic cleaning (e–h). These fouled membranes were fixed, washed, dehydrated, dried, and sputter-coated with gold before SEM observation.

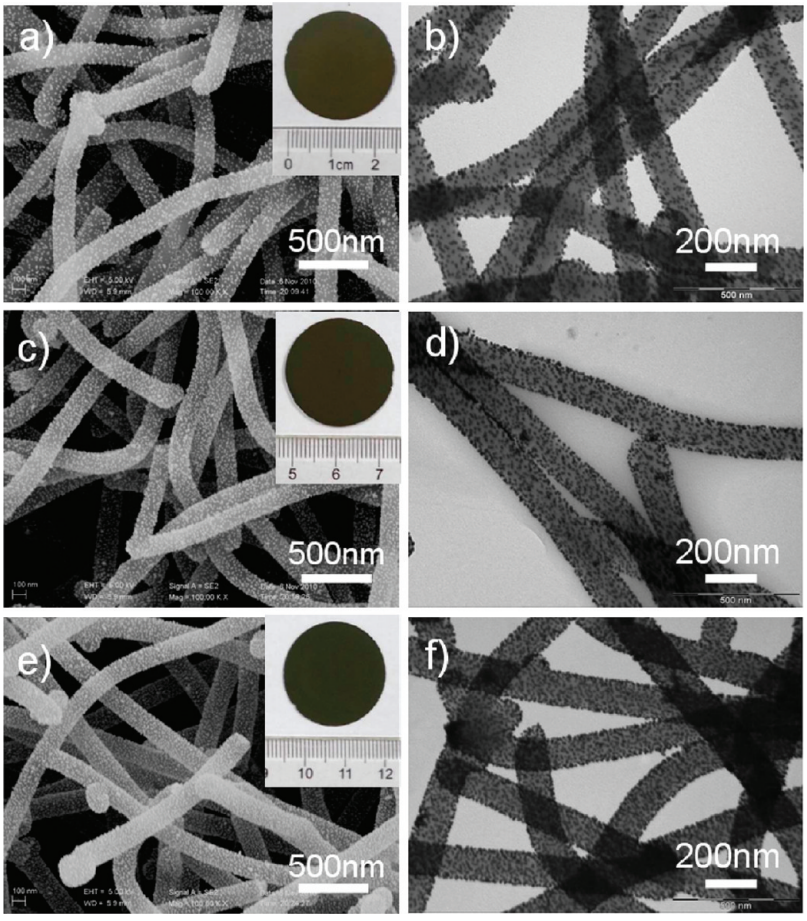

Figure 8. Morphology characterization of CNFs-Au composite nanofibers. SEM and TEM images of CNFs-130-Au-1 (a,b), CNFs-130-Au-2 (c,d), and CNFs-130-Au-3 (e,f) composite nanofibers, which were fabricated by loading 200, 400, and 800 mL of Au colloids solution (0.24 mM) on 100 mg of CNFs-130, respectively. The insets in the SEM images show the photographs of the corresponding CNFs-Au membranes.

The above results undoubtedly indicated that our CNFs-Ag composite nanofibrous membranes exhibit excellent antimicrobial and antibiofouling activities and have great potential as high-performance filters for long-term operation.

CNFs-Au Nanofibrous Membranes as Catalytic Reactors. Finally, we fabricated CNFs-Au composite fibrous membranes by loading AuNPs on the surface of CNFs and examined their catalytic behavior in a continuous-flow mode. AuNPs can readily catalyze various oxidation and reduction reactions. However, the high surface energy of particles in the nanoscale results in aggregation and subsequent decreased catalytic activity. One of the strategies for preventing AuNPs from aggregation was immobilizing the catalytic nanoparticles on a suitable porous membrane to form a catalytic reactor.

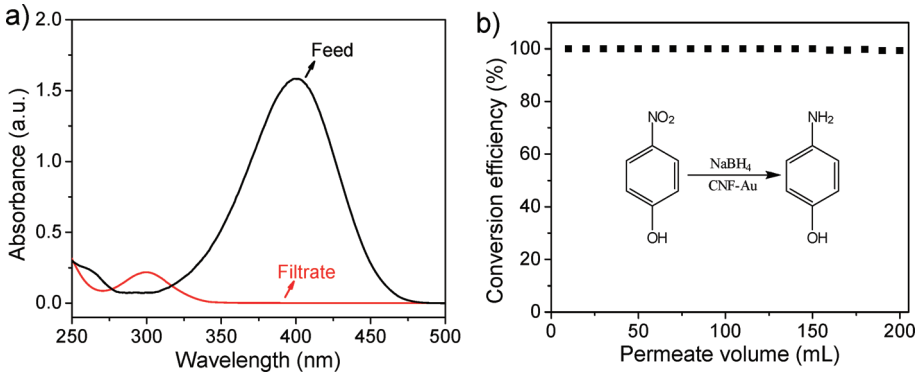

Figure 9. (a) UV−vis absorption spectra of a solution consisting of 0.1 mM 4-nitrophenol and 10 mM $NaBH_4$ before and after passing through the CNFs-Au composite membrane. (b) Plot of percent conversion of 4-nitrophenol to 4-aminophenol against the volume of the solution passing through the CNFs-Au catalytic membrane. The inset shows the scheme of reduction of 4-nitrophenol by $NaBH_4$ when passing through the catalytic membrane. The expected product is 4-aminophenol.

The catalytic membrane reactors combine the conversion effect (catalyst) and separation effect (membrane) in a single unit and have shown several potential benefits, which mainly include allowing for continuous-flow operation, avoiding the separation of the products from reaction system, enhancement of catalytic reaction rate and selectivity, and decreased possibility for the products to run side reactions or poison the catalyst surfaces.[41,42]

The CNFs-Au composite nanofibers were prepared through a two-step route (Scheme 1d). The CNFs were first modified by a saline coupling agent KH-550 since the hydroxylic groups on the CNFs could react with the functionalized silanes. Then, different amounts of ~12 nm Au colloids were loaded on the surface-modified CNFs, which was based on the specific affinity interactions between the gold and the NH_2 groups supplied by the KH-550 on the surface of CNFs. These CNFs-Au composite nanofibers possess terrific active catalyst surfaces because AuNPs were largely and uniformly loaded on the surfaces of the CNF matrix, as shown in the SEM and TEM images (Figure 8). Increasing the amount of Au colloids solution could proportionally increase the loading effect (Figure 8). For example, on the basis of 100 mg of CNFs-130, adding increasingly 200, 400, and 800 mL of the ~12 nm Au colloids solution (0.24 mM Au) resulted in the enhancement of Au loading in the final products from 24.2% (CNFs-130-Au-1) to 39.2% (CNFs-130-Au-2) and then up to 48.6% (CNFs-130-Au-3), determined by the ICP-AES techniques. It is noted that further increasing of the volume of Au solution could not efficiently improve the loading because of saturation of NH_2 groups. These CNFs-Au composite nanofibers were then assembled into corresponding free-standing membranes (the insets in Figure 8a,c,e).

To investigate the catalysis ability of the CNFs-Au composite membrane in a continuous-flow mode, we chose to study the reduction of 4-nitrophenol to its corresponding amino derivatives in the presence of $NaBH_4$, which serves as a rapid and easily characterized model reaction and is well-known that the reaction does not proceed without catalysts (the inset in Figure 9b).[43] The reduction reaction results in the color transformation from yellow to colorless, and we can monitor easily the extent of the reaction and further examine the conversion efficiency using UV−vis spectra. Aqueous solution containing 0.1 mM 4-nitrophenol and 10 mM $NaBH_4$ was passed through the CNFs-Au composite membrane (~50 μm in thickness) and original feed solution and filtered solution samples were analyzed by UV−vis spectra. The original 4-nitrophenol solution showed a strong absorbance maximum at 400 nm, which disappeared in the UV−vis spectrum of the filtered solution. At the same time, a new peak at 290 nm appeared, which was attributed to the 4-aminophenol (Figure 9a).[43] A nearly 100% reduction of the 4-nitrophenol after the passage of the reaction solution through the membrane at a rate of 0.25 mL/min (Figure 9a) clearly demonstrated the obvious catalytic activities of the composite membrane, although the catalytic tests have not been optimized. The control experiment where the Au-free CNF membrane was examined showed no color change occurring after passing the reaction solution, which revealed that the catalytic activity of the CNFs-Au composite membrane came exclusively from the Au sites and the CNFs served only as a scaffold. More importantly, this membrane could maintain >99% conversion of 4-nitrophenol to 4-aminophenol for more than 200 mL of permeate volume (Figure 9b), which corresponds to nearly 10 000 membrane volumes, indicating the persistent catalytic ability of our CNFs-Au composite membrane for long-term.

CONCLUSION

In summary, we have demonstrated that the highly active CNFs could be used as a versatile scaffold for constructing multifunctional free-standing membranes. Benefiting from the highly functionalized

surfaces of the CNFs, a variety of composite nanofibers were prepared by coating different nanoparticles with the desirable properties on the CNF scaffolds, including magnetic particles (CNFs-Fe_3O_4), photocatalyst (CNFs-TiO_2), bacteriostatic agent (CNFs-Ag), and noble metal catalyst (CNFs-Au). These hybrid nanofibers can be assembled into free-standing multifunctional membranes with potential applications in various fields. Particularly, the CNFs-Fe_3O_4 composite membranes can be actuated by a household magnet with reversible deformation and were expected to be used as smart microfluidics devices. By integrating the advanced filtering capabilities of nanofibrous membrane and antimicrobial properties of Ag nanoparticles, we have shown that the CNFs-Ag composite membranes can filtrate out bacteria from water completely and meanwhile exhibit excellent antibiofouling ability. The CNFs-Au composite membranes displayed the persistent catalytic ability in a continuous-flow mode.

Although exemplified here by fabrication and characterization of four CNF-based composite membranes, the versatility of the CNF scaffolds is significantly broad in scope. For example, immobilization of enzyme on CNF scaffolds probably results in free-standing membranes with biosensing or biocatalytic ability.[44] Incorporation of special organic dyes or metallic ions into the CNFs may bring affinity membrane chromatography used for enrichment and separation of biomacromolecules.[45−47] Further study of these possible applications of CNF-based composite membranes is in progress.

METHODS

Materials. Polyvinylpyrrolidone (PVP), sodium tellurite, hydrazine hydrate (85%, w/w %), aqueous ammonia solution (25−28%, w/w %), glucose, H_2O_2 (5%), hydrochloric acid, triethylene glycol (TEG), tetrabutyltitanate, $AgNO_3$, $HAuCl_4 \cdot 3H_2O$, trisodium citrate dihydrate, silane coupling agent KH-550, phosphate buffered saline (PBS), glutaraldehyde, and ethanol were commercially available from Shanghai Chemical Reagent Co. Ltd. Iron(III) acetylacetonate ($Fe(acac)_3$) was purchased from Sigma-Aldrich. All of the chemicals were used without further purification.

Synthesis of Highly Uniform CNF Scaffolds. The first step involved the synthesis of ultrathin Te nanowire templates *via* a simple hydrothermal method.[48] Then the CNFs were prepared by a template-directed hydrothermal carbonization procedure developed by our group recently.[17,18] Briefly, 30 mL of acetone was added into 10 mL of the prepared Te nanowire solution to precipitate the product before centrifuging at 6000 rpm, which was then dispersed into 80 mL of glucose solution (5 g of glucose) with vigorous magnetic stirring for 15 min. Hydrothermal treatment of the mixed solution at 160 °C for different times could result in Te@C nanocables with various diameters. Pure CNFs could be obtained by removal of Te templates by chemical etching in an acidic H_2O_2 solution.

Preparation of CNFs-Fe_3O_4 Composite Nanofibers. The CNFs-Fe_3O_4 composite nanofibers were prepared by thermal decomposition of $Fe(acac)_3$ in TEG in the presence of CNFs. In a typical synthesis, 200 mg of $Fe(acac)_3$ was dissolved in 30 mL of TEG by ultrasonication and magnetic stirring. Then 100 mg of CNFs was dispersed in the above solution by vigorous magnetic stirring. The suspension was then transferred into a Teflon-lined stainless steel autoclave (50 mL in total volume), sealed, and maintained at 220 °C for 12 h. After being cooled to room temperature naturally, the products were diluted by absolute ethanol, centrifuged, and washed several times with absolute ethanol.

Preparation of CNFs-TiO_2 Composite Nanofibers. The CNFs-TiO_2 composite nanofibers were prepared by hydrolysis of tetrabutyltitanate in the presence of CNFs slowly in ethanol. Typically, 0.2 mL of tetrabutyltitanate was dissolved in 20 mL of absolute ethanol to form a mixture solution. Next 50 mg of CNFs was dispersed in this freshly prepared solution with magnetic stirring for 0.5 h. Then 10.0 mL of water/ethanol mixture (H_2O/C_2H_5OH = 0.5:9.5, v/v) was added slowly to the above suspension of CNFs over a period of approximately 10 min with vigorous magnetic stirring. Thereafter, the suspension was stirred for 0.5 h before centrifugation and washing with ethanol. Finally, after hydrothermal treatment of the above products at 180 °C for 12 h, well-defined CNFs-TiO_2 composite nanofibers were yielded.

Preparation of CNFs-Ag Composite Nanofibers. The CNFs-Ag composite nanofibers were prepared through *in situ* reducing of $AgNO_3$ by the hydroxylic groups on CNFs. Briefly, 50 mg of CNFs was dispersed in 20 mL of $AgNO_3$ solution (0.5 M) by vigorous stirring. Then the mixed solution was shaken at a rotation rate of 260 rpm using an Innova 40 benchtop incubator shaker for 12 h at room temperature or 60 °C. The products were collected by centrifugation and washed several times with double-distilled water and absolute ethanol.

Preparation of CNFs-Au Composite Nanofibers. The CNFs-Au composite nanofibers were prepared through a two-step strategy. The first step involved surface modification of CNFs with a saline coupling agent KH-550. Briefly, 100 mg of CNFs was dispersed in 50 mL of ethanol before 50 mL of 20 wt % KH-550 ethanol solution was added. After magnetic stirring (for 1.0 h), centrifuging, and washing with water, the surface-modified CNFs were obtained. The second step involved direct loading of Au nanoparticles on surface-modified CNFs. The modified CNFs was added into 200 mL of ~12 nm Au nanoparticle solution (0.24 mM), which were prepared by the Frens's method.[49] After about 2 min, the adsorption of Au onto the CNFs was totally completed, as the red color of Au nanoparticles faded away quickly. Then the purified CNFs-Au composite nanofibers were yielded after centrifuging and washing.

Fabrication of Multifunctional CNF-Based Composite Membranes. The above CNF-based composite nanofibers, including CNFs-Fe_3O_4, CNFs-TiO_2, CNFs-Ag, and CNFs-Au, could be assembled into corresponding free-standing membranes through a solvent-evaporation-induced self-assembly process.[17] Vigorous magnetic stirring of the CNF-based composite nanofibers in ethanol (or water) for several hours was necessary to form a flocculent homogeneous suspension (5−10 mg/mL). After casting the suspension onto a Teflon substrate and drying at ambient temperature, a free-standing membrane was formed, which could be easily detached from the substrate without any cracking. The colors of the membranes vary for different kinds of CNF-based composites. The thickness of the membranes was dependent on the volume and concentration of suspension.

Antibacterial Tests of the CNFs-Ag Composites. In order to investigate the bactericidal and antibiofouling properties of the CNFs-Ag composite membranes, the wild-type *E. coli* inoculum was prepared by culturing overnight at 37 °C and shaking at 260 rpm in 50 mL of LB broth medium from a single colony surface on LB agar plates. Then about 2 mL of the culture was transferred into 100 mL of fresh LB medium and further conditioned at 37 °C to form the *E. coli* inoculum.

Kinetic Test. For the kinetic test, 5 mL of *E. coli* inoculum was added to 50 mL of fresh LB broth medium containing as-synthesized CNFs-Ag composites with different concentrations (*i.e.*, 25, 50, and 100 μg/mL). The nutrient broth solutions of

bacterial suspensions without any CNFs-Ag composites added and with pure CNFs added were also made as the control. Then 1.0 mL aliquots were withdrawn from the flasks at hourly intervals and were diluted to an appropriate concentration. The concentration of the bacterial suspensions was measured using a UV−vis spectrophotometer at 600 nm.

Zone of Inhibition. For the zone of inhibition test, the Kirby−Bauer technique was used. Briefly, 100 g of sterilized LB media containing 1.5% agar was melted and kept at 50 °C for 30 min. This nutrient agar was poured onto a disposable sterilized Petri dish and was allowed to solidify. Then 100 μL of overnight-cultured *E. coli* (10^6 CFU/mL) was streaked over the plate and was spread uniformly. Circular CNFs-Ag composite membrane and Ag-free CNFs membrane (diameter of ~8 mm) were gently placed over the solidified agar gel in different Petri dishes. The zone of inhibition was observed and measured after incubation for 24 h at 37 °C.

Filtration for Removal of Bacterial Contaminants. The CNFs-Ag membrane was then tested for its ability to remove bacteria from water. The filtration tests were conducted with a dead-end stirred cell (Model 8010, Millpore Co., USA; the volume capacity is 10 mL, and the effective area of the membrane is 4.1 cm^2), which was sterilized prior to the filtration. The CNFs-Ag membranes were cut into a round shape with a diameter of 25 mm and then placed in the cell. A bulk solution of 10 mL of *E. coli* with a load of ~10^6 CFU/mL was prepared in sterilized PBS (0.01 M, pH 7.0) solution. The solution was forced to pass through the prepared CNFs-Ag composite membrane at a constant flow rate (0.5 mL/min) using a peristaltic pump (Model DHL-B, Shanghai Huxi Analysis Instrument Factory Co., Ltd.). The filtrate was taken in sterilized conical flasks. Both the filtrate and the unfiltered bacterial suspension were plated on agar plates and incubated at 37 °C overnight. The number of bacterial colonies was counted to estimate the efficiency of the filtration.

Filtration Protocol for Evaluating the Antibiofouling Properties of CNFs-Ag Membranes. In order to evaluate the antibiofouling properties, 10 mL of *E. coli* with a load of ~10^7 CFU/mL was filtrated through the CNFs-Ag membrane using the Millpore cell. Then the membrane was gently removed out from the cell and incubated on the surface of LB agar plate for 24 h overnight to maximize bacterial growth. After that, the fouled membrane was loaded into the cell again to measure the water flux (J_f) to examine the biofilm formation at a pressure of 40 kPa applied by a N_2 tank. For evaluating the reversible fouling, another fouled CNF-Ag membrane was hydraulically cleaned by soaking in sterilized water and shaking for 30 min at 260 rpm before measuring the water flux (J_h). Ag-free CNF membranes, commercially available mixed cellulose ester (MCE), and polyvinylidene fluoride (PVDF) membranes were also tested as described above for comparison. For each membrane, the clean water flux (J_w) was also measured at the same pressure prior to fouling. For examination of the inhibition of bacterial growth by SEM, another set of membranes after fouling and hydraulic cleaning were fixed in 3 vol % glutaraldehyde in PBS for 5 h at 4 °C. After being washed with PBS, the membranes were dehydrated gradually with 30, 60, 90, and 100% ethanol for 10 min each. Finally, the membranes were dried in air and sputter-coated with a thin layer of gold before SEM observation.

Continuous-Flow Catalytic Tests of the CNFs-Au Composite Membrane. The continuous-flow catalytic tests were conducted with a Millpore cell (Model 8010, the effective area is 4.1 cm^2) at room temperature. Aqueous solution containing 0.1 mM 4-nitrophenol and 10 mM $NaBH_4$ was passed through the membrane at a flux of 0.25 mL/min using a peristaltic pump. Original feed solution and filtered solution samples were analyzed by UV−vis spectrophotometry to determine the extent of the reaction described above and further to examine the conversion efficiency of the composite membrane.

Characterization. Scanning electron microscopy (SEM) was performed with a field emission scanning electron microanalyzer (Zeiss Supra 40). Transmission electron microscopy (TEM) was performed on H-7650 (Hitachi, Japan) operated at an acceleration voltage of 100 kV. X-ray photoelectron spectra (XPS) were recorded on an ESCALab MKΠ X-ray photoelectron spectrometer, using Mg Kα radiation as the excitation source. The UV−vis spectra were recorded on a UV-2501PC/2550 (Shimadzu Corporation, Japan) at room temperature by using $BaSO_4$ as the calibration reagent. X-ray power diffraction (XRD) analyses were carried out on a Philips X'Pert PRO SUPER X-ray diffractometer equipped with graphite-monochromatized Cu Kα radiation. The magnetic properties of the samples were investigated using a superconducting quantum interface device (SQUID) magnetometer (Quantum Design MPMS XL). Inductively coupled plasma atomic emission spectrometry (ICP-AES) measurements were conducted using an Optima 7300 DV spectrometer, PerkinElmer Inc., USA. Inductively coupled plasma mass spectrometry (ICP-MS) measurements were conducted on XSERIES 2, Thermo Fisher Scientific Inc., USA. N_2 adsorption measurements were determined by an ASAP 2020 accelerated surface area and porosimetry (Micromeritics), equipped with automated surface area, at 77 K using Barrett−Emmett−Teller (BET) calculations for surface area.

Acknowledgment. S.H.Y. acknowledges the funding support from the National Basic Research Program of China (2010CB934700), the National Natural Science Foundation of China (Nos. 91022032, 50732006), the International Science & Technology Cooperation Program of China (2010DFA41170), and the Partner-Group of the Chinese Academy of Sciences-the Max Planck Society. H.W.L. acknowledges the funding support from the Fundamental Research Funds for the Central Universities.

Supporting Information Available: Synthesis parameters of the all samples, additional SEM and TEM images of CNFs and CNF-based composite nanofibers, magnetization curves, and XRD patterns. This material is available free of charge *via* the Internet at http://pubs.acs.org.

REFERENCES AND NOTES

1. Davis, V. A.; Parra-Vasquez, A. N. G.; Green, M. J.; Rai, P. K.; Behabtu, N.; Prieto, V.; Booker, R. D.; Schmidt, J.; Kesselman, E.; Zhou, W.; *et al.* True Solutions of Single-Walled Carbon Nanotubes for Assembly into Macroscopic Materials. *Nat. Nanotechnol.* **2009**, *4*, 830–834.
2. Capadona, J. R.; Van Den Berg, O.; Capadona, L. A.; Schroeter, M.; Rowan, S. J.; Tyler, D. J.; Weder, C. A Versatile Approach for the Processing of Polymer Nanocomposites with Self-Assembled Nanofibre Templates. *Nat. Nanotechnol.* **2007**, *2*, 765–769.
3. Wu, Z. C.; Chen, Z. H.; Du, X.; Logan, J. M.; Sippel, J.; Nikolou, M.; Kamaras, K.; Reynolds, J. R.; Tanner, D. B.; Hebard, A. F.; *et al.* Transparent, Conductive Carbon Nanotube Films. *Science* **2004**, *305*, 1273–1276.
4. Zhang, M.; Fang, S. L.; Zakhidov, A. A.; Lee, S. B.; Aliev, A. E.; Williams, C. D.; Atkinson, K. R.; Baughman, R. H. Strong, Transparent, Multifunctional, Carbon Nanotube Sheets. *Science* **2005**, *309*, 1215–1219.
5. Endo, M.; Muramatsu, H.; Hayashi, T.; Kim, Y. A.; Terrones, M.; Dresselhaus, N. S. 'Buckypaper' from Coaxial Nanotubes. *Nature* **2005**, *433*, 476–476.
6. Bryning, M. B.; Milkie, D. E.; Islam, M. F.; Hough, L. A.; Kikkawa, J. M.; Yodh, A. G. Carbon Nanotube Aerogels. *Adv. Mater.* **2007**, *19*, 661–664.
7. Gutierrez, M. C.; Hortiguela, M. J.; Amarilla, J. M.; Jimenez, R.; Ferrer, M. L.; del Monte, F. Macroporous 3D Architectures of Self-Assembled Mwcnt Surface Decorated with Pt Nanoparticles as Anodes for a Direct Methanol Fuel Cell. *J. Phys. Chem. C* **2007**, *111*, 5557–5560.
8. Halonen, N.; Rautio, A.; Leino, A. R.; Kyllonen, T.; Toth, G.; Lappalainen, J.; Kordas, K.; Huuhtanen, M.; Keiski, R. L.; Sapi, A.; *et al.* Three-Dimensional Carbon Nanotube Scaffolds as Particulate Filters and Catalyst Support Membranes. *ACS Nano* **2010**, *4*, 2003–2008.
9. Dong, W. J.; Cogbill, A.; Zhang, T. R.; Ghosh, S.; Tian, Z. R. Multifunctional, Catalytic Nanowire Membranes and the Membrane-Based 3D Devices. *J. Phys. Chem. B* **2006**, *110*, 16819–16822.

10. Yuan, J. K.; Liu, X. G.; Akbulut, O.; Hu, J. Q.; Suib, S. L.; Kong, J.; Stellacci, F. Superwetting Nanowire Membranes for Selective Absorption. *Nat. Nanotechnol.* **2008**, *3*, 332–336.
11. Peng, X. S.; Jin, J.; Ericsson, E. M.; Ichinose, I. General Method for Ultrathin Free-Standing Films of Nanofibrous Composite Materials. *J. Am. Chem. Soc.* **2007**, *129*, 8625–8633.
12. Krogman, K. C.; Lowery, J. L.; Zacharia, N. S.; Rutledge, G. C.; Hammond, P. T. Spraying Asymmetry into Functional Membranes Layer-by-Layer. *Nat. Mater.* **2009**, *8*, 512–518.
13. Teo, W. E.; Ramakrishna, S. Electrospun Nanofibers as a Platform for Multifunctional, Hierarchically Organized Nanocomposite. *Compos. Sci. Technol.* **2009**, *69*, 1804–1817.
14. Olsson, R. T.; Samir, M. A. S. A.; Salazar-Alvarez, G.; Belova, L.; Strom, V.; Berglund, L. A.; Ikkala, O.; Nogues, J.; Gedde, U. W. Making Flexible Magnetic Aerogels and Stiff Magnetic Nanopaper Using Cellulose Nanofibrils as Templates. *Nat. Nanotechnol.* **2010**, *5*, 584–588.
15. Eichhorn, S. J.; Dufresne, A.; Aranguren, M.; Marcovich, N. E.; Capadona, J. R.; Rowan, S. J.; Weder, C.; Thielemans, W.; Roman, M.; Renneckar, S.; *et al.* Review: Current International Research into Cellulose Nanofibres and Nanocomposites. *J. Mater. Sci.* **2010**, *45*, 1–33.
16. Guo, C. X.; Zheng, X. T.; Ng, S. R.; Lai, Y.; Lei, Y.; Li, C. M. *In Situ* Molecular Detection of Ischemic Cells by Enhanced Protein Direct Electron Transfer on a Unique Horseradish Peroxidase-Au Nanoparticles-Polyaniline Nanowires Biofilm. *Chem. Commun.* **2011**, *47*, 2652–2654.
17. Liang, H. W.; Wang, L.; Chen, P. Y.; Lin, H. T.; Chen, L. F.; He, D. A.; Yu, S. H. Carbonaceous Nanofiber Membranes for Selective Filtration and Separation of Nanoparticles. *Adv. Mater.* **2010**, *22*, 4691–4695.
18. Qian, H. S.; Yu, S. H.; Luo, L. B.; Gong, J. Y.; Fei, L. F.; Liu, X. M. Synthesis of Uniform Te@Carbon-Rich Composite Nanocables with Photoluminescence Properties and Carbonaceous Nanofibers by the Hydrothermal Carbonization of Glucose. *Chem. Mater.* **2006**, *18*, 2102–2108.
19. Qian, H. S.; Antonietti, M.; Yu, S. H. Hybrid "Golden Fleece": Synthesis and Catalytic Performance of Uniform Carbon Nanoribers and Silica Nanotubes Embedded with a High Population of Noble-Metal Nanoparticles. *Adv. Funct. Mater.* **2007**, *17*, 637–643.
20. Aulin, C.; Netrval, J.; Wagberg, L.; Lindstrom, T. Aerogels from Nanofibrillated Cellulose with Tunable Oleophobicity. *Soft Matter* **2010**, *6*, 3298–3305.
21. Sun, S. H.; Murray, C. B.; Weller, D.; Folks, L.; Moser, A. Monodisperse FePt Nanoparticles and Ferromagnetic FePt Nanocrystal Superlattices. *Science* **2000**, *287*, 1989–1992.
22. Pu, H. T.; Jiang, F. J. Towards High Sedimentation Stability: Magnetorheological Fluids Based on CNT/Fe_3O_4 Nanocomposites. *Nanotechnology* **2005**, *16*, 1486–1489.
23. Tang, J.; Wang, K.-Y.; Zhou, W. Magnetic Properties of Nanocrystalline Fe_3O_4 Films. *J. Appl. Phys.* **2001**, *89*, 7690–7692.
24. Wan, J.; Cai, W.; Feng, J.; Meng, X.; Liu, E. *In Situ* Decoration of Carbon Nanotubes with Nearly Monodisperse Magnetite Nanoparticles in Liquid Polyols. *J. Mater. Chem.* **2007**, *17*, 1188.
25. Cong, H.-P.; He, J.-J.; Lu, Y.; Yu, S.-H. Water-Soluble Magnetic-Functionalized Reduced Graphene Oxide Sheets: *In Situ* Synthesis and Magnetic Resonance Imaging Applications. *Small* **2010**, *6*, 169–173.
26. Khan, S. U. M.; Al-Shahry, M.; Ingler, W. B. Efficient Photochemical Water Splitting by a Chemically Modified N-TiO_2. *Science* **2002**, *297*, 2243–2245.
27. Wang, Y. M.; Du, G. J.; Liu, H.; Liu, D.; Qin, S. B.; Wang, N.; Hu, C. G.; Tao, X. T.; Jiao, J.; Wang, J. Y.; *et al.* Nanostructured Sheets of Ti-O Nanobelts for Gas Sensing and Antibacterial Applications. *Adv. Funct. Mater.* **2008**, *18*, 1131–1137.
28. Qiao, Y.; Bao, S.-J.; Li, C. M.; Cui, X.-Q.; Lu, Z.-S.; Guo, J. Nanostructured Polyaniline/Titanium Dioxide Composite Anode for Microbial Fuel Cells. *ACS Nano* **2007**, *2*, 113–119.
29. Zhu, Y.; Lu, W.; Sun, Z.; Kosynkin, D. V.; Yao, J.; Tour, J. M. High Throughput Preparation of Large Area Transparent Electrodes Using Non-functionalized Graphene Nanoribbons. *Chem. Mater.* **2011**, *23*, 935–939.
30. Pan, J. H.; Zhang, X. W.; Du, A. J.; Sun, D. D.; Leckie, J. O. Self-Etching Reconstruction of Hierarchically Mesoporous F-TiO_2 Hollow Microspherical Photocatalyst for Concurrent Membrane Water Purifications. *J. Am. Chem. Soc.* **2008**, *130*, 11256–11257.
31. Shannon, M. A.; Bohn, P. W.; Elimelech, M.; Georgiadis, J. G.; Marinas, B. J.; Mayes, A. M. Science and Technology for Water Purification in the Coming Decades. *Nature* **2008**, *452*, 301–310.
32. Van der Bruggen, B.; Vandecasteele, C.; Van Gestel, T.; Doyen, W.; Leysen, R. A Review of Pressure-Driven Membrane Processes in Wastewater Treatment and Drinking Water Production. *Environ. Prog.* **2003**, *22*, 46–56.
33. Costerton, J. W.; Lewandowski, Z.; Caldwell, D. E.; Korber, D. R.; Lappinscott, H. M. Microbial Biofilms. *Annu. Rev. Microbiol.* **1995**, *49*, 711–745.
34. Malaisamy, R.; Berry, D.; Holder, D.; Raskin, L.; Lepak, L.; Jones, K. L. Development of Reactive Thin Film Polymer Brush Membranes To Prevent Biofouling. *J. Membr. Sci.* **2010**, *350*, 361–370.
35. Kidambi, S. Investigation of Metal Nanoparticles Encapsulated in Polyelectrolyte Multilayers for Catalytic and Antibacterial Applications. Ph.D. Thesis, Michigan State University, 2007; pp 68−95.
36. Sharma, V. K.; Yngard, R. A.; Lin, Y. Silver Nanoparticles: Green Synthesis and Their Antimicrobial Activities. *Adv. Colloid Interface Sci.* **2009**, *145*, 83–96.
37. Liang, H. W.; Cao, X.; Zhou, F.; Cui, C. H.; Zhang, W. J.; Yu, S. H. A Free-Standing Pt-Nanowire Membrane as a Highly Stable Electrocatalyst for the Oxygen Reduction Reaction. *Adv. Mater.* **2011**, *23*, 1467–1471.
38. Zodrow, K.; Brunet, L.; Mahendra, S.; Li, D.; Zhang, A.; Li, Q. L.; Alvarez, P. J. J. Polysulfone Ultrafiltration Membranes Impregnated with Silver Nanoparticles Show Improved Biofouling Resistance and Virus Removal. *Water Res.* **2009**, *43*, 715–723.
39. Gupta, A.; Maynes, M.; Silver, S. Effects of Halides on Plasmid-Mediated Silver Resistance in *Escherichia coli*. *Appl. Environ. Microbiol.* **1998**, *64*, 5042–5045.
40. Sondi, I.; Salopek-Sondi, B. Silver Nanoparticles as Antimicrobial Agent: A Case Study on *E. coli* as a Model for Gram-Negative Bacteria. *J. Colloid Interface Sci.* **2004**, *275*, 177–182.
41. Julbe, A.; Farrusseng, D.; Guizard, C. Porous Ceramic Membranes for Catalytic Reactors—Overview and New Ideas. *J. Membr. Sci.* **2001**, *181*, 3–20.
42. Dotzauer, D. M.; Dai, J. H.; Sun, L.; Bruening, M. L. Catalytic Membranes Prepared Using Layer-by-Layer Adsorption of Polyelectrolyte/Metal Nanoparticle Films in Porous Supports. *Nano Lett.* **2006**, *6*, 2268–2272.
43. Hayakawa, K.; Yoshimura, T.; Esumi, K. Preparation of Gold−Dendrimer Nanocomposites by Laser Irradiation and Their Catalytic Reduction of 4-Nitrophenol. *Langmuir* **2003**, *19*, 5517–5521.
44. Yu, A.; Liang, Z.; Caruso, F. Enzyme Multilayer-Modified Porous Membranes as Biocatalysts. *Chem. Mater.* **2004**, *17*, 171–175.
45. Ma, Z. W.; Kotaki, M.; Ramakrishna, S. Electrospun Cellulose Nanofiber as Affinity Membrane. *J. Membr. Sci.* **2005**, *265*, 115–123.
46. Jain, P.; Sun, L.; Dai, J.; Baker, G. L.; Bruening, M. L. High-Capacity Purification of His-Tagged Proteins by Affinity Membranes Containing Functionalized Polymer Brushes. *Biomacromolecules* **2007**, *8*, 3102–3107.
47. Saxena, A.; Tripathi, B. P.; Kumar, M.; Shahi, V. K. Membrane-Based Techniques for the Separation and Purification of Proteins: An Overview. *Adv. Colloid Interface Sci.* **2009**, *145*, 1–22.
48. Qian, H. S.; Yu, S. H.; Gong, J. Y.; Luo, L. B.; Fei, L. F. High-Quality Luminescent Tellurium Nanowires of Several Nanometers in Diameter and High Aspect Ratio Synthesized by a Poly(vinyl pyrrolidone)-Assisted Hydrothermal Process. *Langmuir* **2006**, *22*, 3830–3835.
49. Frens, G. Controlled Nucleation for the Regulation of the Particle Size in Monodisperse Gold Suspensions. *Nat. Phys. Sci.* **1973**, *241*, 20–23.